Biointerface Research in Applied Chemistry
Open-Access Journal (ISSN: 2069-5837)

Article
Volume 16, Issue 1, 2026, 39
https://doi.org/10.33263/BRIAC161.039

AI-Guided Identification of a Stable MDM2 Mutant for Enhanced Inhibitor Binding in CLL

Ishika Bhoumick [1], Eshika Purkayastha [1], Vedika Pokhrel [1], Vinod Kumar Yata [2,*], Venkata Satish Kumar Mattaparthi [1,*]

[1] Molecular Modeling and Simulation Laboratory, Department of Molecular Biology and Biotechnology, Tezpur University, Tezpur, Assam, 784028, India; ishikakoj@gmail.com (I.B.); eshika.purkayastha2704@gmail.com (E.P.); pokhrelvedika@gmail.com (V.P.); mvenkatasatishkumar@gmail.com (V.S.K.M.), venkata@tezu.ernet.in (V.S.K.M.);
[2] Department of Pharmacology, School of Allied Healthcare Sciences, Malla Reddy University, Hyderabad, Telangana, 500100, India; vinod.kumaryata@mallareddyuniversity.ac.in;
* Correspondence: venkata@tezu.ernet.in (V.S.K.M.); vinod.kumaryata@mallareddyuniversity.ac.in (V.K.Y.);

Received: 6.05.2025; Accepted: 27.10.2025; Published: 15.02.2026

Abstract: Chronic lymphocytic leukemia (CLL) is characterized by the overproduction of lymphocytes and frequently involves MDM2 overexpression, which impairs p53 tumor suppressor activity. Nutlin-3A, a small-molecule inhibitor, binds to MDM2's p53-binding site, preventing this interaction. In this study, the stability of MDM2 mutations at the 86th residue was evaluated using ThermoMPNN, identifying Y86R as a stable mutant with a ΔΔG of -0.9922 kcal/mol. Structural modeling and docking using UCSF ChimeraX and CB-Dock2 revealed enhanced binding of Nutlin-3A to the Y86R mutant (docking score: –9.2 kcal/mol) compared to wild-type MDM2 (–8.5 kcal/mol). Molecular dynamics simulations (50 ns) further supported this finding, showing comparable RMSD (~1.0 Å) and compact Rg values (12.75–13.1 Å) for both complexes. These results suggest that the Y86R mutation may increase Nutlin-3A binding affinity and support its potential utility in CLL cases with MDM2 dysregulation. Overall, this study provides valuable insights into MDM2 inhibition strategies for targeted CLL therapy.

Keywords: MDM2; Nutlin-3A; thermoMPNN; thermostable mutants; molecular simulation; docking; binding affinity.

1. Introduction

The World Health Organization (WHO) classified chronic lymphocytic leukemia (CLL) in 2008 as a lymphoproliferative disease that involves monomorphic round B lymphocytes in bone marrow (BM), lymphoid organs, and peripheral blood (PB) [1,2]. The clonal growth and accumulation of mature, usually CD5-positive B-cells in the spleen, bone marrow, lymph nodes, and blood are its defining characteristics. These B-cells have apoptosis resistance. B-cell chronic lymphocytic leukemia (CLL) is the most prevalent type of lymphoid cancer in Western nations, making up 25% of all leukemias [3]. DNA breaks activate the transcription factor p53, which can cause cell-cycle arrest or apoptosis. p53 preserves the integrity of the genome and stops the spread of clones by coordinating the repair or destruction of cells with damaged DNA [4-6]. MDM2 overexpression has been reported to be a potential cause of p53 dysfunction in CLL. MDM2, a p53-specific E3 ubiquitin ligase, regulates the

ubiquitin-dependent degradation of p53 and is a major cellular antagonist of p53. Overexpression of MDM2, which can increase tumorigenic potential and resistance to apoptosis, has been found in 50% to 70% of CLL patients [7]. Thus, MDM2 is a transcriptional target of p53, establishing an autoregulatory loop: p53 induces *MDM2* gene expression, and MDM2, in turn, leads to p53 inactivation and degradation [8]. In cells with p53, Nutlins, which are strong and specific small-molecule antagonists of MDM2, bind MDM2 in the p53-binding pocket and trigger the p53 pathway. Additionally, it has been reported that Nutlins can trigger p53 signaling without p53 phosphorylation. As a result, Nutlins may be able to reverse the functional p53 inactivation linked to MDM2 overexpression in CLL [9,10].

The purpose of this research is to examine the molecular processes that underlie the therapeutic effectiveness of MDM2 inhibitors, especially in relation to mutations linked to CLL. The Protein Data Bank (PDB)structure with ID 4HG7, which denotes the wild-type MDM2 protein, was used in this study. The stability of the mutant MDM2 structure was assessed using the ThermoMPNN (message-passing neural network) tool, and the mutant structure was generated using the visualization tool UCSF ChimeraX Version 1.9. Subsequently, molecular docking was performed using the CB-Dock2 platform, and the results were analysed to determine the binding affinities and interaction profiles of Nutlin-3A with wild-type and mutant MDM2 structures. Molecular Dynamics Simulations were performed using the AMBER software package. In this study, we focused on methods to aid in the development of more potent CLL treatments by clarifying the inhibitor's binding properties to MDM2 protein structures.

2. Materials and Methods

2.1. Preparation of initial structures.

The 3-D structure of wild-type MDM2 protein bound with Nutlin-3A complex (PDB ID: 4HG7) was retrieved from RCSB PDB (https://www.rcsb.org/) [11]. The 3-D structure of the wild-type MDM2 protein was retrieved by separating the complex from the ligand using UCSF ChimeraX version 1.9 [12] (Figure 1A). The ligand structure Nutlin-3A of ID: 11433190 was taken from the PubChem database (https://pubchem.ncbi.nlm.nih.gov/) [13,14], ensuring that it was in its most stable and relevant form for docking (Figure 1C).

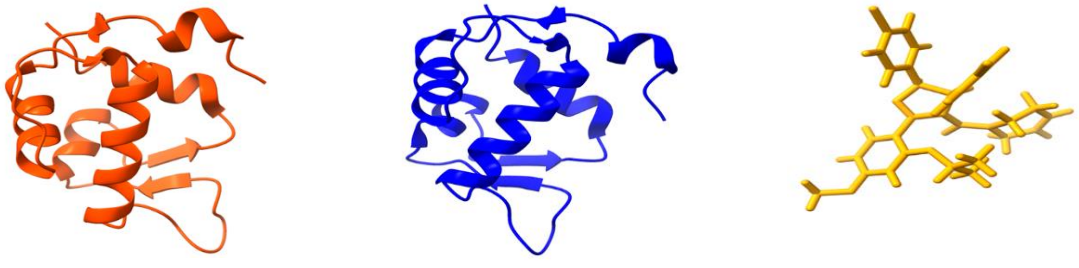

(a) **(b)** **(c)**

Figure 1. Initial structures **(a)** Snapshot of the wild-type MDM2 protein structure taken using UCSF ChimeraX (version 1.9); **(b)** Snapshot of the mutant MDM2-Y86R protein structure made by mutating the 86th position of the wild-type MDM2 protein using UCSF ChimeraX (version 1.9); **(c)** Snapshot of the ligand Nutlin-3A taken using UCSF ChimeraX (version 1.9).

2.2. Identification of stable mutant MDM2 protein using ThermoMPNN.

The stability of various mutations at possible positions of the wild-type MDM2 protein was assessed using the ThermoMPNN tool [15-17] within the Google Colab environment [18,19]. Stability predictions for all mutants were performed using ThermoMPNN, which

provided ΔΔG values, the mutation position, the wild-type amino acid (wtAA), and the mutant amino acid (mutAA). Among the various mutations analysed, the Y86R mutation was selected based on its ΔΔG value of -0.9922 kcal/mol, which was the lowest and indicates the highest predicted stability as shown in Table 1. This systematic computational approach ensured reliable stability rankings and informed the selection of the mutant MDM2-Y86R protein for subsequent structural and functional analyses. Subsequently, the Tyr86 residue of the wild-type MDM2 protein was mutated to Arg86 using UCSF ChimeraX (version 1.9) to generate the mutant MDM2-Y86R protein structure (Figure 1B).

Table 1. Predicted stability changes (ΔΔG) for mutation at possible positions of the MDM2 protein, along with the corresponding wild-type (wtAA) and mutant (mtAA) amino acids.

Mutation	ΔΔG Value (kcal/mol)	wtAA	mtAA
Y86R	-0.9922	Y	R
Q6L	-0.9317	Q	L
Q6M	-0.7170	Q	M
Y86K	-0.6985	Y	K
G65I	-0.6852	G	I
G65F	-0.6804	G	F
S72W	-0.6446	S	W
Q54P	-0.6237	Q	P
S72Y	-0.5825	S	Y
V90E	-0.5352	V	E

2.3. Molecular docking.

Docking was conducted using CB-Dock2 [20, 21] to explore the interactions between the wild-type MDM2 protein and the mutant MDM2-Y86R protein structure with its ligand Nutlin-3A. The protein structures, along with the ligand, were uploaded to the CB-Dock2 web server. CB-Dock2 identified binding cavities in the mutant protein and performed a docking simulation for the ligand, using default parameters to ensure reproducibility. With an emphasis on the binding poses with the lowest docking scores, the docking results were examined to ascertain the ligand's binding affinities and orientations within the designated cavities. Using molecular visualization tools to visualize the docking poses enabled evaluation of key interactions between the protein and ligand, including hydrophobic and hydrogen-bonding interactions. This thorough docking study contributed to additional structural and functional research by providing insights into the binding properties and potential efficacy of Nutlin-3A with the mutant MDM2-Y86R protein.

2.4. Molecular dynamics simulation.

The selected ligand, Nutlin-3A, was curated in xleap using the antechamber procedure. This covered bcc charge addition, FRCMOD file generation, and preparation of complex systems in explicit and implicit solvation. After that, distinct coordinate files and topologies were made for each system. We employed explicit solvation to run MD simulations on the complex system. The wild-type MDM2 protein and mutant MDM2-Y86R protein with ligand Nutlin-3A were subjected to MD simulations. We performed the Molecular Dynamics (MD) simulations using the AMBER ff99SB force field with the AMBER software package [22]. We added an appropriate number of counterions (Na^+ and Cl^- ions) to maintain the two complexes' overall neutrality for this MD simulation. The TIP3PBOX water model [23] was used to solvate the complexes with a solvent buffer of 10 Å in all directions. In the first minimization step, we fixed the complexes by applying harmonic restraints with a force constant of 500 kcal/mol/$Å^2$

and allowed all water molecules and counterions to undergo energy minimization using 2000 steps of steepest descent (SD) followed by 1000 steps of conjugate gradient (CG). Afterwards, in the second step of minimization, the entire complex system was subjected to 5000 steps of SD minimization and 4500 steps of CG minimization to remove any strong van der Waals interactions. Then, the two complexes were gradually heated from 0 to 300 K in constant-volume (NVT) conditions, applying harmonic restraints with a force constant of 10 kcal/mol/Å2 to the solute atoms. Then equilibration was performed thrice for both the complexes with 3000 ps using a force constant of 5.0 kcal/mol/$Å^2$. Lastly, we used an NPT ensemble without restraints to perform 50 ns MD simulations. The Particle mesh Ewald technique [24] was used with a non-bonded cut-off of 12.0 Å to limit the direct space sum. This technique was executed to treat the long-range electrostatic interactions. To constrain all of the system's bonds, we used the SHAKE algorithm. According to Berendsen's weak coupling algorithm [25], we kept the pressure and temperature (0.5 ps of heat bath and 0.2 ps of pressure relaxation) constant throughout the simulation. The time step of the MD simulation was set to 2 fs, and sampling was performed every 10 ps into the MD file. The snapshots for wild-type MDM2-Nutlin-3A complex and mutant MDM2-Y86R-Nutlin-3A complex at a discrete time interval of 10 ns during the course of 50 ns of MD simulation are shown in Figures S1 and S2, respectively.

3. Results and Discussion

3.1. Predicted stability changes.

The stability of various mutations at the 86^{th} position of the MDM2 protein was assessed using the ThermoMPNN tool. ThermoMPNN evaluated the stability of potential mutations, providing a ΔΔG (kcal/mol) score for each mutation. The results are summarised in Table 2, listing the mutations, their corresponding ΔΔG values, the mutation position, the wild-type amino acid (wtAA), and the mutant amino acid (mutAA). The negative ΔΔG value for the Y86R mutation suggests that this mutation stabilizes the MDM2 protein, making it potentially more resilient to misfolding compared to other mutations. This enhanced stability could translate into better functional performance of the MDM2 protein in individuals carrying the Y86R mutation, providing a rationale for further experimental validation. In contrast, most other mutations resulted in positive ΔΔG values, indicating destabilization of the MDM2 protein. For instance, mutations such as Y86P (ΔΔG = 1.61 kcal/mol) and Y86D (ΔΔG = 1.040 kcal/mol) show significant destabilizing effects, likely leading to impaired protein function. These results highlight the critical importance of the Tyr86 residue in maintaining MDM2 protein stability and function. It is noted that the Y86R mutation was computationally generated as a hypothetical variant to explore enhanced Nutlin-3A binding, rather than derived from known clinical observations. We have conducted an additional search in publicly available cancer genomics databases, including COSMIC and cBioPortal. Currently, there is no evidence of the Y86R mutation being reported in CLL patient samples, either as a germline or somatic mutation.

Further structural and functional analyses are necessary to confirm the implications of these computational predictions. Understanding the molecular basis of MDM2 stability and the effects of specific mutations can guide the development of targeted therapies to correct MDM2 overexpression in CLL patients.

Table 2. Predicted stability changes (ΔΔG) for mutations at the 86th position of the MDM2 protein, along with the corresponding wild-type (wtAA) and mutant (mutAA) amino acids.

Mutation	ΔΔG (kcal/mol)	Position	wtAA	mtAA
Y86A	0.1286	86	Y	A
Y86C	-0.0497	86	Y	C
Y86D	1.0401	86	Y	D
Y86E	0.7275	86	Y	E
Y86F	-0.0113	86	Y	F
Y86G	0.8455	86	Y	G
Y86H	0.1529	86	Y	H
Y86I	-0.0637	86	Y	I
Y86K	-0.6985	86	Y	K
Y86L	-0.1392	86	Y	L
Y86M	-0.2055	86	Y	M
Y86N	0.3959	86	Y	N
Y86P	1.61	86	Y	P
Y86Q	-0.0347	86	Y	Q
Y86R	**-0.9922**	**86**	**Y**	**R**
Y86S	0.2825	86	Y	S
Y86T	0.2841	86	Y	T
Y86V	0.0367	86	Y	V
Y86W	0.008	86	Y	W
Y86Y	0	86	Y	Y

3.2. Docking score.

Table 3 represents the result of molecular docking simulations for the MDM2 inhibitor Nutlin-3A with both wild-type MDM2 and mutant MDM2-Y86R protein structures. The docking scores obtained with AutoDock Vina, as well as the ligand's cavity volumes and docking coordinates, are provided. The docking scores indicate the binding affinity of the ligand towards the MDM2 protein. Nutlin-3A demonstrated a docking score of -8.5 kcal/mol for the wild-type MDM2 protein. For the mutant MDM2-Y86R protein, the docking scores were slightly altered with -9.2 kcal/mol. These scores suggest that Nutlin-3A has a high predicted binding affinity for the mutant MDM2-Y86R protein compared to the wild-type. Moreover, the cavity volumes calculated for each docking pose provide insights into the size of the binding pocket occupied by the ligands. Interestingly, despite variations in the docking scores, the cavity volumes remained consistent for the ligand with both wild-type MDM2 and mutant MDM2-Y86R structures. This suggests that the size of the binding pocket does not significantly affect the ligand's binding affinity. We acknowledge that the observed improvement in binding affinity for the Y86R mutant toward Nutlin-3A (~0.7 kcal/mol) is quantitatively modest. However, even small changes in binding free energy can be biologically meaningful in the context of protein–ligand interactions, as they may influence selectivity and functional efficacy. It is important to recognize the limitations of molecular docking scores, which do not always correlate directly with in vivo or in vitro biological potency and are sensitive to the scoring functions employed. Additionally, the 50 ns molecular dynamics simulations used in this study may not fully capture long-timescale conformational dynamics that could influence binding. These limitations should be taken into account when interpreting the binding energy estimations presented here.

Table 3. Docking scores, cavity volumes, and docking coordinates for Nutlin-3A with wild-type MDM2 and mutant MDM2-Y86R structures.

Ligand	Vina score (kcal/mol)		Cavity volume (Å^3)	Centre (x,y,z)	Docking size (x,y,z)
	Wild-type MDM2	Mutant MDM2-Y86R			
Nutlin-3A	-8.5	-9.2	543	-25, 8, -12	23, 23, 23

The spatial orientation of the ligands within the binding site is revealed by the docking coordinates. Each ligand's docking sizes (x, y, z) were consistent between the wild-type and mutant MDM2 structures, suggesting comparable binding postures. This implies that the MDM2 inhibitor's binding mechanism is not significantly changed by the structural alterations brought about by the Y86R mutation. All things considered, these findings imply that Nutlin-3A is a potentially effective treatment option for CLL, as it has the highest anticipated binding affinity for both wild-type and mutant MDM2-Y86R proteins. To verify these computational predictions and assess the effectiveness of this inhibitor in clinical settings, additional experimental validation is needed.

Figure 2 uses surface and hidden receptor images to illustrate the molecular interactions between Nutlin-3A and both wild-type MDM2 and mutant MDM2-Y86R structures. Surface images of the wild-type MDM2 and mutant MDM2-Y86R structures are shown in Figure 2A and 2C, respectively. These images offer a thorough understanding of the ligand's spatial arrangement inside the MDM2 protein's binding pocket. The surface representation highlights the regions of interaction between Nutlin-3A and the protein surface, offering insights into the ligand's binding mode and potential binding pockets. By visualizing the surface interactions, we can observe any notable differences in the binding patterns between wild-type MDM2 and mutant Y86R structures. Notably, the structural rearrangements caused by the Y86R mutation may alter the availability or accessibility of certain binding sites, potentially influencing the ligand’s binding affinity. In contrast, Figures 2B and 2D present hidden receptor images, where the protein structure is displayed as a transparent surface, allowing for a focused view of the ligand-binding site. This visualization method highlights the ligand's location within the protein's binding pocket and demonstrates specific interactions between Nutlin-3A and key MDM2 residues. These images help identify important molecular interactions by concealing the receptor surface, which makes it easier to analyse the ligand's spatial orientation and arrangement within the binding site.

Particular attention should be paid to hydrogen bonding, hydrophobic contacts, and electrostatic interactions between Nutlin-3A and amino acid residues within the binding site. These interactions play a crucial role in stabilizing the ligand-protein complex and could potentially be altered by the mutation. Additionally, the comparison of the mutant Y86R and wild-type MDM2 structures reveals possible changes in the ligand-binding dynamics brought on by the mutation. For instance, in the mutant structure (Figures 2C and 2D), the Y86R substitution may induce subtle shifts in the ligand’s binding pose, which could affect the overall efficacy of Nutlin-3A as a therapeutic agent. Designing more efficient methods to restore MDM2 function in patients with the Y86R mutation requires an understanding of these variations. These results also highlight the importance of considering mutations such as Y86R when developing customized therapies, as they may affect the ligand-binding mechanism and the overall effectiveness of the medication. Table 4 summarizes Nutlin-3A's interaction patterns with the wild-type MDM2 and mutant MDM2-Y86R structures, where the particular MDM2 protein residues that make contact with the ligand during molecular docking are listed.

Table 4. Contact residues of Nutlin-3A with wild-type MDM2 and mutant MDM2-Y86R structures.

Ligand	Contact residues	
	Wild-type MDM2	**Mutant MDM2-Y86R**
Nutlin-3A	GLN18 ILE19 GLN24 LYS51 LEU54 PHE55 LEU57 GLY58 GLN59 ILE61 MET62 TYR67 GLN72 HIS73 VAL75 PHE86 PHE91 VAL93 LYS94 GLU95 HIS96 ILE99 TYR100 ILE103	ILE19 GLN24 MET50 LYS51 GLU52 LEU54 PHE55 LEU57 GLY58 GLN59 ILE61 MET62 TYR67 GLN72 HIS73 ILE74 VAL75 LEU82 PHE86 PHE91 VAL93 LYS94 GLU95 HIS96 ILE99 TYR100 ILE103

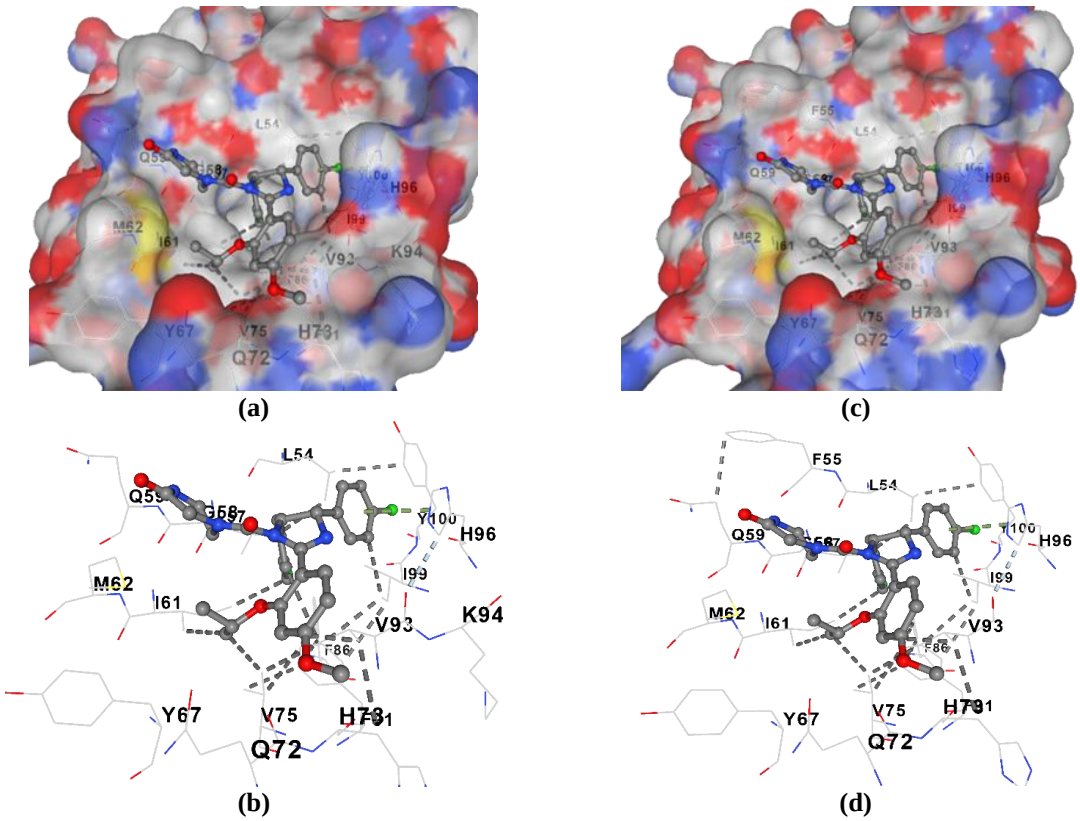

Figure 2. Surface and hidden receptor image, **(a)** Surface image of wild-type MDM2 with ligand Nutlin-3A shows the spatial arrangement of Nutlin-3A inside the binding pocket of wild-type MDM2 protein; **(b)** Hidden receptor image of wild-type MDM2 with ligand Nutlin-3A demonstrates the particular interactions between Nutlin-3A and the wild-type MDM2 protein residues; **(c)** Surface image of mutant MDM2-Y86R with ligand Nutlin-3A shows the spatial arrangement of Nutlin-3A inside the binding pocket of mutant MDM2-Y86R protein; **(d)** Hidden receptor image of mutant MDM2-Y86R with ligand Nutlin-3A demonstrates the particular interactions between Nutlin-3A and the mutant MDM2-Y86R protein.

For the inhibitor Nutlin-3A, several key residues were identified in both wild-type MDM2 and mutant MDM2-Y86R structures. These include ILE19, GLN24, LEU57, GLY58, GLN59, and others. Notably, the contact residues largely overlap between the wild-type and mutant structures, suggesting that the Y86R mutation does not significantly alter the binding interactions of Nutlin-3A with MDM2. Overall, the observed interaction profiles suggest that Nutlin-3A forms stable complexes with both wild-type MDM2 and mutant MDM2-Y86R structures through interactions with specific amino acid residues within the protein. These findings provide valuable insights into the molecular mechanisms underlying the therapeutic efficacy of MDM2 inhibitors and may aid in the rational design of novel therapeutic agents for CLL. Further experimental studies are warranted to validate these computational predictions and elucidate the precise molecular interactions underlying this inhibitor's activity. Overall, these findings provide valuable insights into the molecular mechanisms that may contribute to Nutlin-3A's therapeutic activity in CLL. To verify these computer predictions and investigate this inhibitor's potential in clinical settings, more experimental validation is required.

Although our study primarily focuses on Nutlin-3A and the Y86R mutant, previous research has identified several other MDM2 residues—such as Y100, L54, and F91—as being critical for modulating ligand binding and structural flexibility [26-29]. These residues are known to influence the conformation of the p53-binding cleft and affect the interaction of MDM2 with a variety of small-molecule inhibitors. By comparing our results with these well-characterized mutations and inhibitor interactions, we can see that the Y86R mutation contributes to subtle yet potentially functionally relevant shifts in binding affinity. This broader

comparative framework enhances our understanding of MDM2's structural plasticity and underscores the potential for fine-tuning MDM2–ligand interactions through targeted mutation or drug optimization. Collectively, these insights position our findings within the wider landscape of MDM2-targeted drug discovery and rational inhibitor design.

3.3. MD simulation of wild-type MDM2-Nutlin-3A and mutant MDM2-Y86R-Nutlin-3A complex stuctures.

To study the dynamic properties of the two complexes, wild-type MDM2-Nutlin-3A and mutant MDM2-Y86R-Nutlin-3A, we carried out 50 ns of molecular dynamics simulation.

3.3.1. Root mean square deviation (RMSD) analysis.

Molecular dynamics simulation is a technique used to determine how atoms and molecules move over a specified amount of time. The difference between the backbones of a protein from its initial structural conformation to its final position is measured using the root mean square deviation, or RMSD. The variations created throughout the simulation process can be used to assess the protein's stability in relation to its conformation. The protein structure is more stable when the variations are fewer. To verify the stability of wild-type MDM2-Nutlin-3A complex and the mutant MDM2-Y86R-Nutlin-3A complex, the RMSD value for the C-alpha backbone was computed for a 50 ns simulation of both complexes. From the RMSD plot (Figure 3), it can be observed that the wild-type and mutant complex systems showed overall stability over 50 ns of simulation time.

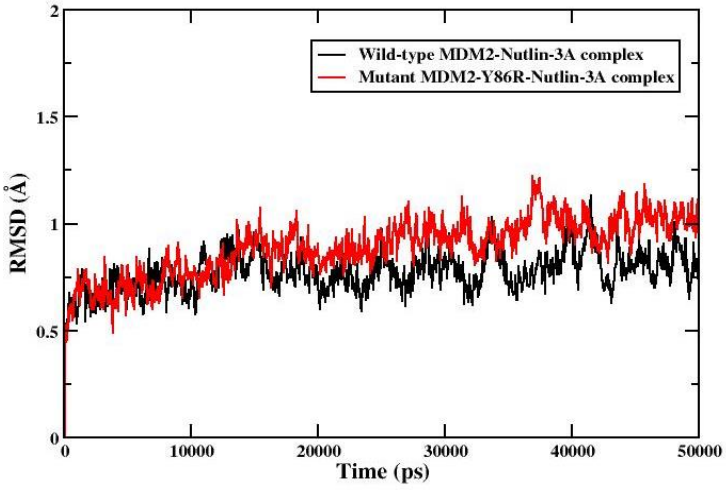

Figure 3. RMSD plot. Both wild-type MDM2-Nutlin-3A complex and mutant MDM2-Y86R-Nutlin-3A complex are stable throughout the 50 ns simulation.

3.3.2. Root mean square fluctuations (RMSF) analysis.

The RMSF of each residue's Cα atoms with respect to their initial position were measured and plotted against the protein residues in order to estimate the conformational flexibility of the protein-ligand complexes. From the RMSF plot of wild-type MDM2-Nutlin-3A complex and the mutant MDM2-Y86R-Nutlin-3A complex (Figure 4), it can be observed that the wild-type complex system and mutant variant complex system exhibit stability and do not show any significant flexibility throughout the simulation.

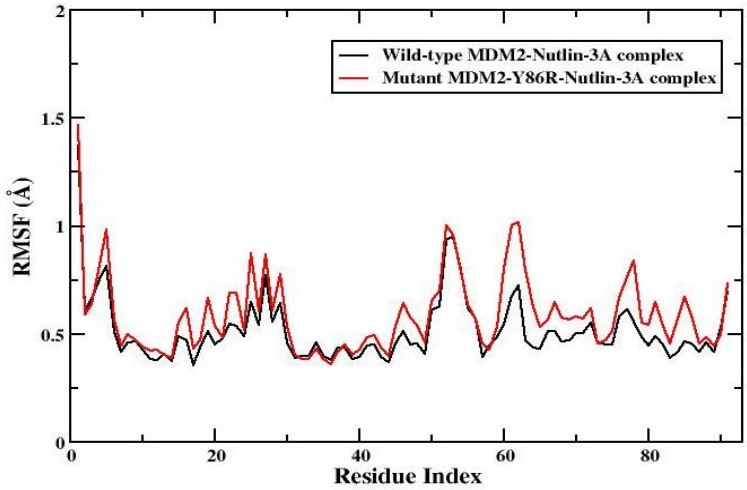

Figure 4. RMSF plot. Both wild-type MDM2-Nutlin-3A complex and mutant MDM2-Y86R-Nutlin-3A complex are stable throughout the 50ns simulation.

3.3.3. Radius of gyration (Rg) analysis.

The Rg plot is a useful metric for evaluating the structural compactness of proteins during interactions with molecules. This indicates the flexibility of a molecule by detecting changes in its shape and size over time. The Rg plot of wild-type MDM2/mutant MDM2-Y86R protein with its ligand Nutlin-3A is shown in Figure 5. The Rg values in both the wild-type and mutant variant complexes range from 12.75 to 13.1 Å, indicating that the complexes are compact and tightly bound.

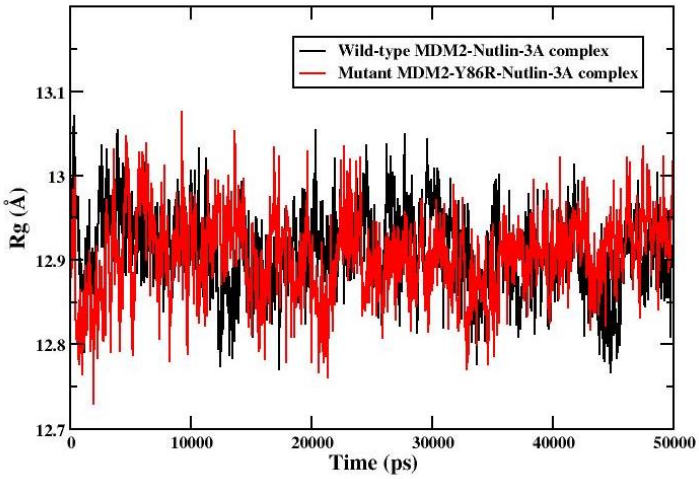

Figure 5. Rg plot. Both wild-type MDM2-Nutlin-3A complex and mutant MDM2-Y86R-Nutlin-3A complex are stable throughout the 50 ns simulation, as both complexes are compact and tightly bound.

3.3.4. Solvent accessible surface area (SASA) analysis.

SASA is a measure of the surface area of a protein that is accessible to the solvent molecules. The change in the SASA was analysed to measure the compactness of the hydrophobic core. SASA is typically calculated by methods involving the in-silico rolling of a spherical probe, which approximates a water molecule, around a full-atom protein model. Higher scores mean that more of the molecule is sticking out into water, and lower scores mean that more of the molecule is buried in the protein. Therefore, proteins with higher SASA values have more surface area exposed to solvent, which can make them more flexible and more

amenable to drug binding. In the SASA plot of wild-type MDM2/mutant MDM2-Y86R protein with their ligand, Nutlin-3A (Figure 6), we observe fluctuations in both complexes, indicating dynamic changes in solvent exposure.

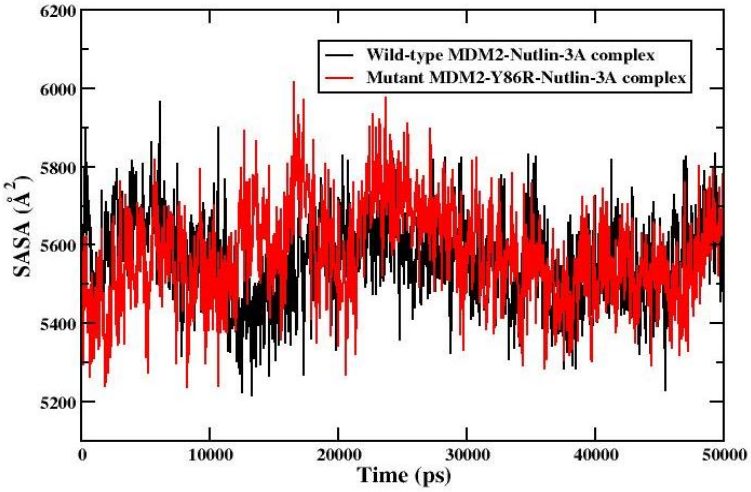

Figure 6. SASA plot. Both wild-type MDM2-Nutlin-3A complex and mutant MDM2-Y86R-Nutlin-3A complex are stable throughout the 50ns simulation. Higher SASA values indicate more solvent exposure, while lower values suggest a more compact structure.

4. Conclusion

In conclusion, our molecular docking and molecular dynamics simulations reveal that Nutlin-3A exhibits the highest predicted binding affinity with a score of -9.2 kcal/mol for the mutant MDM2-Y86R protein. This finding suggests that Nutlin-3A has a lot of potential as a treatment for people with Y86R-mutant Chronic Lymphocytic Leukemia (CLL). Nutlin-3A's strong, stable binding affinity for both wild-type and mutant MDM2-Y86R structures highlights its potential to target the disease's underlying molecular pathways. To confirm these computational results and investigate the potential clinical use of Nutlin-3A in the treatment of CLL, more experimental research is necessary.

Author Contributions

Conceptualization, I.B. and V.S.K.M.; methodology, I.B.; formal analysis, I.B. and E.P.; writing—original draft preparation, I.B. and V.P.; writing—review and editing, E.P., V.K.Y., and V.S.K.M.; supervision, V.K.Y. and V.S.K.M. All authors have read and agreed to the published version of the manuscript.

Institutional Review Board Statement

Not applicable.

Informed Consent Statement

Not applicable.

Data Availability Statement

The data supporting the findings of the study are available within the article.

Funding

This research received no external funding.

Acknowledgments

The authors extend their deepest gratitude to Tezpur University and the University Grants Commission, India, for the start-up grant.

Conflicts of Interest

The authors declare no conflict of interest.

Abbreviations

The following abbreviations are used in this manuscript:

Abbreviation	Definition
CLL	Chronic Lymphocytic Leukemia
MDM2	Murine Double-Minute 2
MPNN	Message-Passing Neural Network
RCSB PDB	Research Collaboratory for Structural Bioinformatics Protein Data Bank
CB-Dock2	Cavity Detection-guided Docking version 2

References

1. Scarfò, L.; Ferreri, A.J.; Ghia, P. Chronic lymphocytic leukaemia. *Crit. Rev. Oncol. Hematol.* **2016**, *104*, 169-82, https://doi.org/10.1016/j.critrevonc.2016.06.003.
2. Bosch, F.; Dalla-Favera, R. Chronic lymphocytic leukaemia: from genetics to treatment. *Nat. Rev. Clin. Oncol.* **2019**, *16*, 684-701, https://doi.org/10.1038/s41571-019-0239-8.
3. Shanafelt, T.D.; Ghia, P.; Lanasa, M.C.; Landgren, O.; Rawstron, A.C. Monoclonal B-cell lymphocytosis (MBL): biology, natural history and clinical management. *Leukemia* **2010**, *24*, 512-520, https://doi.org/10.1038/leu.2009.287.
4. Lin, K.; Sherrington, P.D.; Dennis, M.; Matrai, Z.; Cawley, J.C.; Pettitt, A.R. Relationship between p53 dysfunction, CD38 expression, and IgV(H) mutation in chronic lymphocytic leukemia. *Blood* **2002**, *100*, 1404-1409, https://doi.org/10.1182/blood-2001-11-0066.
5. Vogelstein, B.; Lane, D.; Levine, A.J. Surfing the p53 network. *Nature* **2000**, *408*, 307-310, https://doi.org/10.1038/35042675.
6. Brooks, C.L.; Gu, W. p53 ubiquitination: Mdm2 and beyond. *Mol. Cell.* **2006**, *21*, 307-315, https://doi.org/10.1016/j.molcel.2006.01.020.
7. Harris, S.L.; Levine, A.J. The p53 pathway: positive and negative feedback loops. *Oncogene* **2005**, *24*, 2899-2908, https://doi.org/10.1038/sj.onc.1208615.
8. Mayr, C.; Bund, D.; Schlee, M.; Bamberger, M.; Kofler, D.M.; Hallek, M.; Wendtner, C.M. MDM2 is recognized as a tumor-associated antigen in chronic lymphocytic leukemia by $CD8^+$ autologous T lymphocytes. *Exp. Hematol.* **2006**, *34*, 44-53, https://doi.org/10.1016/j.exphem.2005.09.016.
9. Kojima, K.; Konopleva, M.; McQueen, T.; O'Brien, S.; Plunkett, W.; Andreeff, M. Mdm2 inhibitor Nutlin-3a induces p53-mediated apoptosis by transcription-dependent and transcription-independent mechanisms and may overcome Atm-mediated resistance to fludarabine in chronic lymphocytic leukemia. *Blood* **2006**, *108*, 993-1000, https://doi.org/10.1182/blood-2005-12-5148.
10. Drakos, E.; Thomaides, A.; Medeiros, L.J.; Li, J.; Leventaki, V.; Konopleva, M.; Andreeff, M.; Rassidakis, G.Z. Inhibition of p53-murine double minute 2 interaction by nutlin-3A stabilizes p53 and induces cell cycle arrest and apoptosis in Hodgkin lymphoma. *Clin. Cancer Res.* **2007**, *13*, 3380-3387, https://doi.org/10.1158/1078-0432.CCR-06-2581.
11. Berman, H.M.; Westbrook, J.; Feng, Z.; Gilliland, G.; Bhat, T.N.; Weissig, H.; Shindyalov, I.N.; Bourne, P.E. The Protein Data Bank. *Nucleic Acids Res.* **2000**, *28*, 235-242, https://doi.org/10.1093/nar/28.1.235.

12. Pettersen, E.F.; Goddard, T.D.; Huang, C.C.; Meng, E.C.; Couch, G.S.; Croll, T.I.; Morris, J.H.; Ferrin, T.E. UCSF ChimeraX: Structure visualization for researchers, educators, and developers. *Protein Sci.* **2021**, *30*, 70-82, https://doi.org/10.1002/pro.3943.
13. Kim, S. Getting the most out of PubChem for virtual screening. *Expert Opin. Drug Discov.* **2016**, *11*, 843-55, https://doi.org/10.1080/17460441.2016.1216967.
14. Wang, Y.; Xiao, J.; Suzek, T.O.; Zhang, J.; Wang, J.; Zhou, Z.; Han, L.; Karapetyan, K.; Dracheva, S.; Shoemaker, B.A.; Bolton, E.; Gindulyte, A.; Bryant, S.H. PubChem's BioAssay Database. *Nucleic Acids Res.* **2012**, *40*, D400-12, https://doi.org/10.1093/nar/gkr1132.
15. Dauparas, J.; Anishchenko, I.; Bennett, N.; Bai, H.; Ragotte, R.J.; Milles, L.F.; Wicky, B.I.M.; Courbet, A.; de Haas, R.J.; Bethel, N.; Leung, P.J.Y.; Huddy, T.F.; Pellock, S.; Tischer, D.; Chan, F.; Koepnick, B.; Nguyen, H.; Kang, A.; Sankaran, B.; Bera, A.K.; King, N.P.; Baker, D. Robust deep learning-based protein sequence design using ProteinMPNN. *Science* **2022**, *378*, 49-56, https://doi.org/10.1126/science.add2187.
16. Cock, P.J.; Antao, T.; Chang, J.T.; Chapman, B.A.; Cox, C.J.; Dalke, A.; Friedberg, I.; Hamelryck, T.; Kauff, F.; Wilczynski, B.; de Hoon, M.J. Biopython: freely available Python tools for computational molecular biology and bioinformatics. *Bioinformatics* **2009**, *25*, 1422-3, https://doi.org/10.1093/bioinformatics/btp163.
17. Dieckhaus, H.; Brocidiacono, M.; Randolph, N.Z.; Kuhlman, B. Transfer learning to leverage larger datasets for improved prediction of protein stability changes. *Proc. Natl. Acad. Sci. U S A* **2024**, *121*, e2314853121, https://doi.org/10.1073/pnas.2314853121.
18. Ganesan, S.; Mittal, N.; Bhat, A.; Adiga, R.S.; Ganesan, A.; Nagarajan, D.; Varadarajan, R. Improved Prediction of Stabilizing Mutations in Proteins by Incorporation of Mutational Effects on Ligand Binding. *Proteins* **2025**, *93*, 384-395, https://doi.org/10.1002/prot.26738.
19. Vallejo, W.; Díaz-Uribe, C.; Fajardo, C. Google Colab and Virtual Simulations: Practical e-Learning Tools to Support the Teaching of Thermodynamics and to Introduce Coding to Students. *ACS Omega* **2022**, 7, 7421-7429, https://doi.org/10.1021/acsomega.2c00362.
20. Liu, Y.; Grimm, M.; Dai, W.T.; Hou, M.C.; Xiao, Z.X.; Cao, Y. CB-Dock: a web server for cavity detection-guided protein-ligand blind docking. *Acta Pharmacol. Sin.* **2020**, *41*, 138-144, https://doi.org/10.1038/s41401-019-0228-6.
21. Liu, Y.; Yang, X.; Gan, J.; Chen, S.; Xiao, Z.X.; Cao, Y. CB-Dock2: improved protein-ligand blind docking by integrating cavity detection, docking and homologous template fitting. *Nucleic Acids Res* **2022**, *50*, W159-W164, https://doi.org/10.1093/nar/gkac394.
22. Case, D.A.; Cheatham III, T.E.; Darden, T.; Gohlke, H.; Luo, R.; Merz Jr., K.M.; Onufriev, A.; Simmerling, C.; Wang, B.; Woods, R.J. The Amber biomolecular simulation programs. *J. Comput. Chem.* **2005**, *26*, 1668-88, https://doi.org/10.1002/jcc.20290.
23. Jorgensen, W.L.; Chandrasekhar, J.; Madura, J.D.; Impey, R.W.; Klein, M.L. Comparison of Simple Potential Functions for Simulating Liquid Water. *J. Phys. Chem. Lett.* **1983**, *79*, 926−935, https://doi.org/10.1063/1.445869.
24. Darden, T.; York, D.; Pedersen, L. Particle Mesh Ewald: An N·Log (N) Method for Ewald Sums in Large Systems. *J. Phys. Chem. Lett.* **1993**, *98*, 10089-10092, https://doi.org/10.1063/1.464397.
25. Berendsen, H.J.; Postma, J.V.; Van, G.W.F.; Dinola, A.R.H.; Haak, J.R. Molecular Dynamics with Coupling to an External Bath. *J. Comput. Phys.* **1984**, *81*, 3684-3690, https://doi.org/10.1063/1.448118.
26. Dastidar, S.G.; Lane, D.P.; Verma, C.S. Modulation of p53 binding to MDM2: computational studies reveal important roles of Tyr100. *BMC Bioinformatics* **2009**, *10*, S6. https://doi.org/10.1186/1471-2105-10-S15-S6.
27. Showalter, S.A.; Bruschweiler-Li, L.; Johnson, E.; Zhang, F.; Brüschweiler, R. Quantitative Lid Dynamics of MDM2 Reveals Differential Ligand Binding Modes of the p53-Binding Cleft. *J. Am. Chem. Soc.* **2008**, *130*, 6472–6478, https://doi.org/10.1021/ja800201j.
28. Kussie, P.H.; Gorina, S.; Marechal, V.; Elenbaas, B.; Moreau, J.; Levine, A.J.; Pavletich, N.P. Structure of the MDM2 Oncoprotein Bound to the p53 Tumor Suppressor Transactivation Domain. *Science* **1996**, *274*, 948–953, https://doi.org/10.1126/science.274.5289.948.
29. Das, P.; Mattaparthi, V.S.K. Computational Investigation on the p53–MDM2 Interaction Using the Potential of Mean Force Study. *ACS Omega* **2020**, *5*, 8449–8462, https://doi.org/10.1021/acsomega.9b03372.

Publisher's Note & Disclaimer

Supplementary Materials

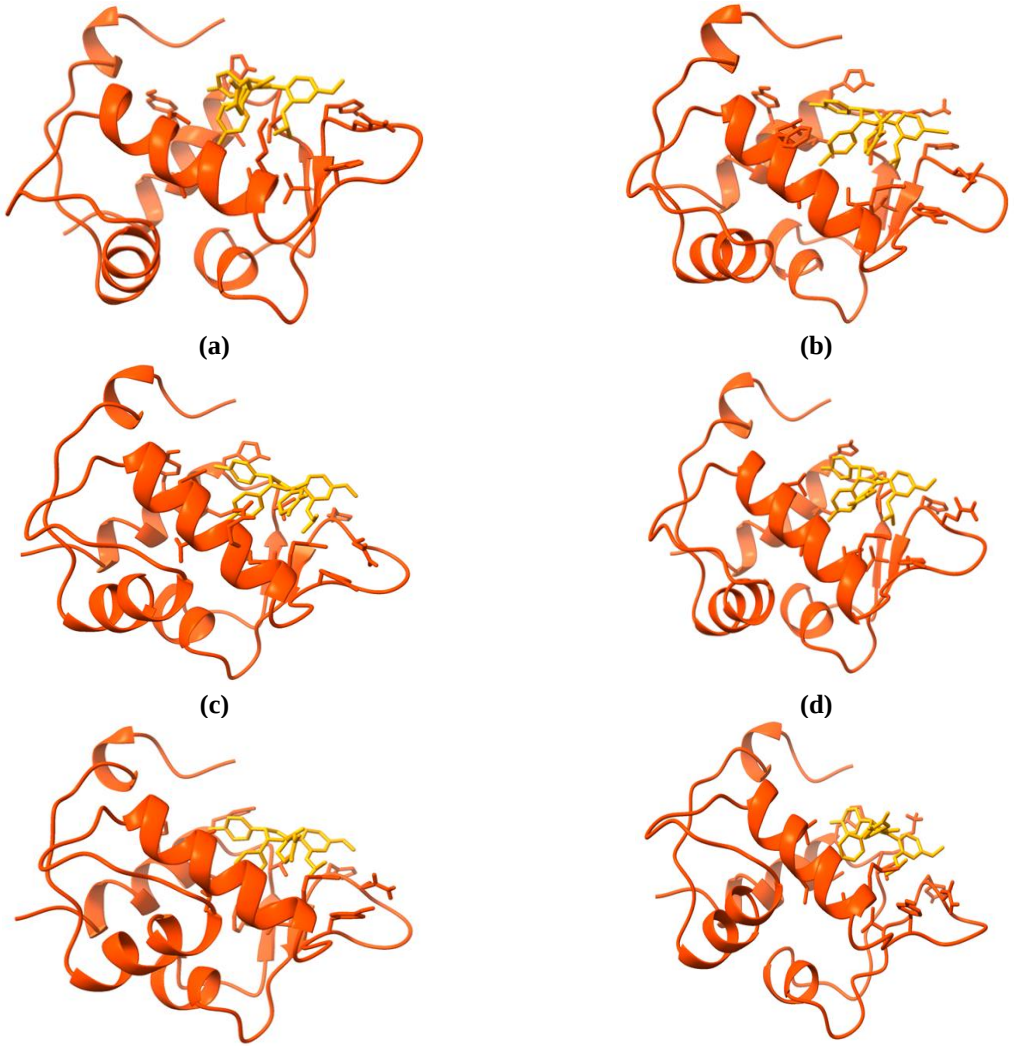

(a) **(b)** **(c)** **(d)** **(e)** **(f)**

Figure S1. Snapshots of wild-type MDM2-Nutlin-3A complex structures at discrete time intervals of **(a)** 0; **(b)** 10; **(c)** 20; **(d)** 30; **(e)** 40; **(f)** 50 ns of MD simulation.

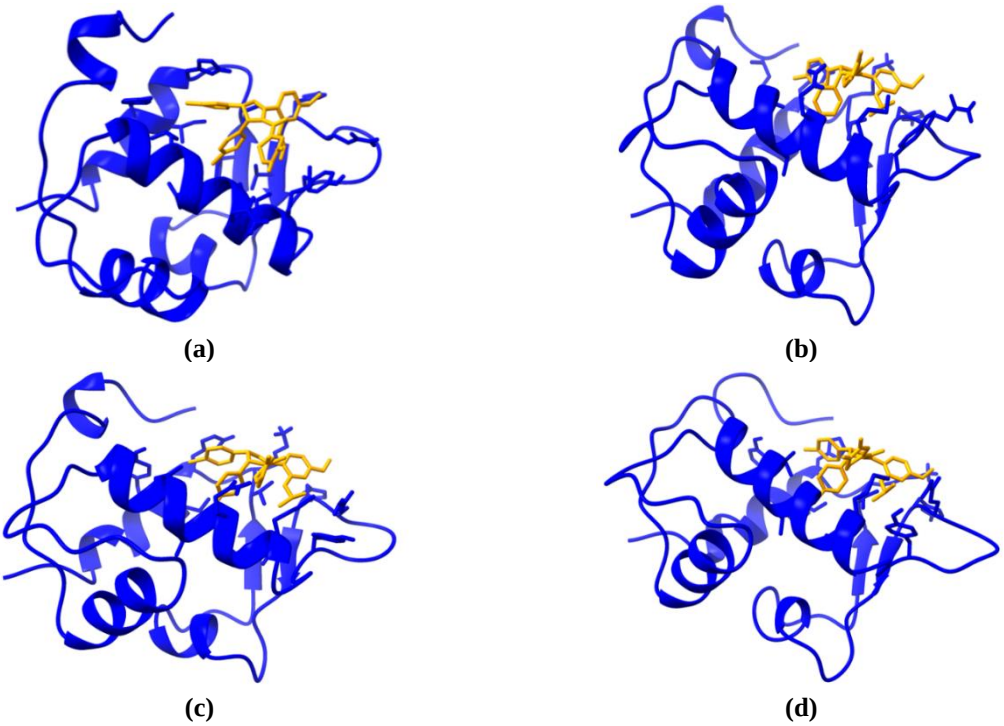

(a) **(b)** **(c)** **(d)**

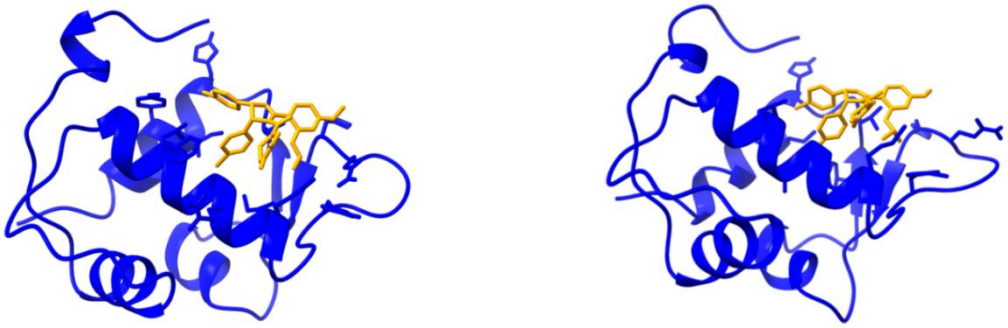

(e) **(f)**

Figure S2. Snapshots of mutant MDM2-Y86R-Nutlin-3A structures at discrete time intervals of **(a)** 0; **(b)** 10; **(c)** 20; **(d)** 30; **(e)** 40; **(f)** 50 ns of MD simulation.